ISSN (Print) 1226-1750
ISSN (Online) 2233-6656
Journal of Magnetics 18(3), 283-288 (2013) http://dx.doi.org/10.4283/JMAG.2013.18.3.283

Topology Design Optimization of Electromagnetic Vibration Energy Harvester to Maximize Output Power

Jaewook Lee[1]* and Sang Won Yoon[2]

[1]*School of Aerospace and Mechanical Engineering, Korea Aerospace University, Goyang, Gyeonggi-do 412-791, Korea*
[2]*Department of Electrical Engineering and Computer Science, University of Michigan, Ann Arbor, MI 48109, USA*

(Received 8 May 2013, Received in final form 29 July 2013, Accepted 2 August 2013)

This paper presents structural topology optimization that is being applied for the design of electromagnetic vibration energy harvester. The design goal is to maximize the root-mean-square value of output voltage generated by external vibration leading structures. To calculate the output voltage, the magnetic field analysis is performed by using the finite element method, and the obtained magnetic flux linkage is interpolated by using Lagrange polynomials. To achieve the design goal, permanent magnet is designed by using topology optimization. The analytical design sensitivity is derived from the adjoint variable method, and the formulated optimization problem is solved through the method of moving asymptotes (MMA). As optimization results, the optimal location and shape of the permanent magnet are provided when the magnetization direction is fixed. In addition, the optimization results including the design of magnetization direction are provided.

Keywords : topology design optimization, energy harvesting, finite element methods

1. Introduction

Energy harvesters capture and stores energy from the environment, and are expected to be used as clean and renewable power sources for various applications including wireless sensor networks and wearable electronics [1, 2]. Vibration energy harvesters rely on mechanical structures which respond to environment vibration [2]. The mechanical structures commonly have natural frequencies tuned to vibration frequencies which are dominantly observed in target applications to maximize the energy-conversion efficiency [1, 2]. In the electromagnetic energy harvesters, the resonating structure changes magnetic flux generated from (integrated) permanent magnet (PM) so that the time variation of the magnetic flux induces the voltage which is picked up by coils, according to Faraday's law [3]. Thus, the designs of the resonating structures, PM and pick-up coils are the key to electromagnetic energy harvesters.

For outstanding performances on electromagnetic vibration energy harvesters, considerable efforts have been investigated. A single energy harvester has multiple PMs that induce multi-directional magnetic flux change [4, 5]. Multiple harvesters are arrayed to increase output voltages by summing up voltage from each harvester, or to increase bandwidth by differing from each harvester's natural frequency [6, 7]. Recent studies reported advanced energy-conversion mechanisms including the frequency up-conversion [3, 6, 8] and hybrid mechanisms [9, 10]. In addition, new magnetic materials developed by micro-/nano-technologies are actively investigated [11].

One challenge for energy harvesters is determining the optimal shapes and locations of their elements (i.e. PM, pick-up coils etc.). Topology optimization [12] has been established as a promising approach to identify the optimal structures of various electromagnetic devices, which includes linear actuators [13, 14], electric motors [15], and piezo-electric energy harvesters [16]. In addition, the application of topology optimization for the design of PM shapes and magnetization directions has been reported in [17] and [18]. However, the topology optimization approach has not been employed in the design of electromagnetic energy harvesters. A few works reported a parametric study which analyzes the location and dimensions of a freely moving PM passing through a pick-up coil [19], but the optimization approach including the design of PM shapes and magnetization directions has not been presented although it highly affects the performances of electromagnetic energy harvesters.

Accordingly, this work presents a topology optimization approach that improves the performance of electromagnetic energy harvesters. The main performance of the harvester is

*Corresponding author: Tel: +82-2-300-0290
Fax: +82-2-3158-2123, e-mail: wookslee@kau.ac.kr

the generated output power, which can be calculated from the root-mean-square (RMS) value of the output voltage curve. To maximize the output power, the RMS value of the voltage is maximized by using the topology optimization approach. This approach facilitates notable enhancements of harvester performances by optimizing locations, shapes, and magnetization directions of PM, and thus, does not require innovative technologies such as state-of-the-art materials or novel conversion mechanisms. In addition, the optimal design in various magnetization direction of PM is investigated, and the design of magnetization direction itself is also provided. The paper is organized as follows. Section II describes an electromagnetic energy harvester design used in this paper and explains the performance analysis to predict the output voltage curve. Using the analysis, the topology design optimization process is presented in section III. The optimization result is provided in section IV. Section V summarizes the paper.

2. Performance Analysis

The structure of electromagnetic energy harvesters used in this work is shown in Fig. 1. Among eight structure types in literatures are classified in [20], this work selects magnet-in-line structure (i.e. the oscillation direction is in-line with the coil symmetry axis) without back iron. In this type, a PM is directly connected with the spring, and thus, works as the mass of the vibration systems. The PM oscillates towards a coil, and thus, the time variation of magnetic fields generates the voltage in the coil.

Through performance analysis, the conversion of vibration energy to electrical energy can be modeled. First, the vibration analysis gives the maximum displacement of harvester moving part. Then, the magnetic flux linkage at various locations of moving parts is calculated by using the finite element analysis. Finally, the output voltage of the energy harvester is evaluated by considering electromagnetic induction. For the performance analysis, the energy harvester

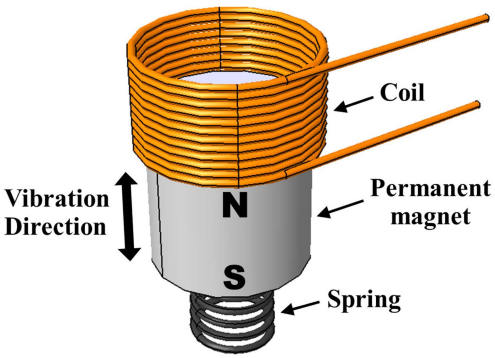

Fig. 1. (Color online) Structure of electromagnetic energy harvesters used in this work (Magnet-in-line without back-iron type).

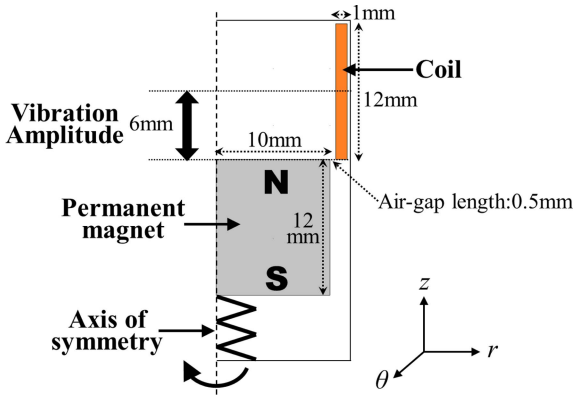

Fig. 2. (Color online) Initial design in a two-dimensional axi-symmetric model.

in Fig. 1 is simplified into two-dimensional axisymmetric model as shown in Fig. 2. The locations and dimensions of initial design are also presented in Fig. 2.

2.1. Vibration analysis

The vibration analysis processes of the energy harvester are similar to that of passive vibration isolators, which is shown in Fig. 3. Thus, the lumped model to represent the displacement of the mass $x(t)$ can be employed as:

$$m\ddot{x} = k(y - x) + c(\dot{y} - \dot{x}) \tag{1}$$

which consists of mass m, spring stiffness k, damping factor c, and displacement of external vibration $y(t)$. When the external vibration $y(t)$ is assumed to be harmonic with the amplitude Y (i.e. $y(t)=Y\sin(\omega t)$), the $x(t)$ of (1) can be solved to be:

$$x(t) = X\sin(\omega t - \phi) \tag{2}$$

$$X = Y \cdot \sqrt{\frac{1 + (2\zeta \cdot \omega/\omega_n)}{(1 - (\omega/\omega_n)^2)^2 + (2\zeta \cdot \omega/\omega_n)^2}} \tag{3}$$

$$\phi = \tan^{-1}\left(\frac{2\zeta \cdot \omega/\omega_n}{1 - (\omega/\omega_n)^2}\right) \tag{4}$$

which consists of natural frequency of undamped oscillation $\omega_n = \sqrt{k/m}$, damping factor $\zeta = c/(2\sqrt{km})$. The resonance frequency maximizing X is $\omega_d = \omega_n\sqrt{1-2\zeta^2}$. By matching the resonance frequency ω_d with the external vibration frequency ω, the displacement of mass is maximized, and consequently, it maximizes the output power of energy harvester. In this work, ω_n, ζ, and Y is set as 1000 Hz, 0.021, and 2.5 μm, respectively. Therefore, the frequency ω and corresponding maximum displacement of mass (X) is fixed to be 1000 Hz and 6 mm, respectively. These values are calculated by representing the recent trend of encapsulated energy harvesters in vacuum to

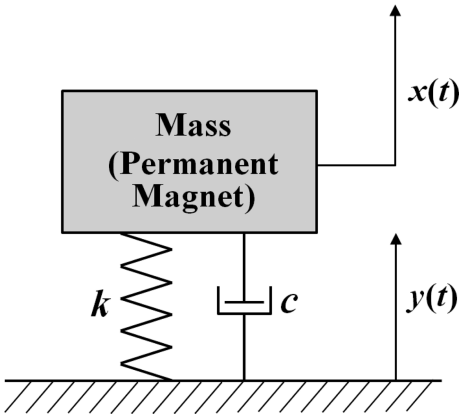

Fig. 3. Spring-mass-damper model for vibration analysis.

achieve high quality factor (Q) and large vibration-induced mass displacement (X) [21]. Vacuum encapsulation readily provides a large Q in the range of a few thousands to a few tens of thousands, as observed in resonating MEMS devices.

2.2. Flux linkage calculation

The next step is to find flux linkages during the mass movements. It is calculated from the magnetic field distribution, which is available by solving Maxwell's equation for low-frequency applications:

$$\nabla \times (\nu \nabla \times \mathbf{A}) = \nabla \times (\nu \mathbf{B}_{\text{residual}}) \tag{5}$$

where ν is magnetic reluctivity, $\mathbf{A}$ is the magnetic vector potential, and $\mathbf{B}_{\text{residual}}$ is the residual magnetic flux density of the PM. The above Eq. (5) is solved by the finite element method when using the commercial software COMSOL v3.5. The mass movement is automatically executed by controlling the material properties using MATLAB. The distributions of magnetic flux density $\mathbf{B}$ ($=\nabla \times \mathbf{A}$) at various mass locations gives the flux linkage Φ_i at ith mass location as:

$$\Phi_i = \frac{1}{S_{coil}} \int 2\pi r A_\theta dS \tag{6}$$

where S_{coil} is the sectional area of coil, r is distance from axis of symmetry, and A_θ is θ-directional component of magnetic vector potential $\mathbf{A}$.

2.3. Output voltage calculation

The output voltage $\varepsilon(t)$ (i.e. electromotive force) is calculated by Faraday's law of induction:

$$\varepsilon(t) = -\frac{d\Phi(t)}{dt} \tag{7}$$

The continuous function $\Phi(x)$ is firstly built from flux linkages Φ_i at discrete mass locations x_i using Lagrange polynomials:

$$\Phi(x) = \sum_i L_i(x)\Phi_i \left(L_i(x) = \prod_{\substack{j=0 \\ j \neq i}} \frac{x - x_j}{x_i - x_j} \right) \tag{8}$$

From (2), (7) and (8) and chain rule, the output voltage ε can be derived as:

$$\varepsilon(t) = -\frac{d\Phi(x)}{dt} \cdot \frac{dx}{dt} = -\left[\sum_i \frac{L_i(x(t))}{dx} \Phi_i \right] \cdot \omega X \cos(\omega t - \phi) \tag{9}$$

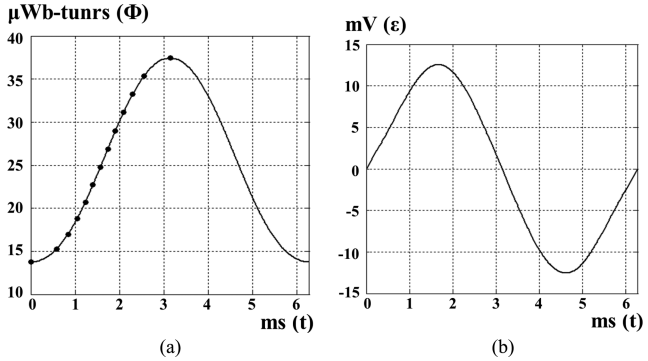

Fig. 4. (a) Flux linkage curves Φ(t), (b) Output voltage curves ε(t) of initial design (Fig. 2).

Fig. 4 shows the calculated flux linkage function $\Phi(t)$ and corresponding output voltage $\varepsilon(t)$ of initial design. The black dots in Fig. 4(a) represent discrete flux linkages Φ_i. This interpolation based analysis method waives the assumption that the flux linkage curve could be sinusoidal, and thus, it can represent any complex shapes of flux linkage curves.

3. Topology Design Optimization

This section explains the topology optimization approach for the design of the energy harvester. First, the optimization problem is formulated. The interpolation functions for material properties using the density method are presented for topology optimization. Next, the design sensitivity analysis is derived using the adjoint variable method.

3.1. Optimization problem formulation

The design goal is to maximize the root-mean-square (RMS) value of output voltage ε_{rms} during the oscillation of energy harvester. To achieve this design goal, the optimization problem is formulated as:

$$\text{Find } \rho_1 \text{ and } \rho_2 \tag{10}$$

$$\text{Maximize } \varepsilon_{\text{rms}} \tag{11}$$

$$\text{Subject to } \mathbf{K}(\rho_1)\mathbf{A}_\theta = \mathbf{f}(\rho_1, \rho_2) \tag{12}$$

$$V_{\mathrm{PM}}(\rho_1) = V^*_{\mathrm{PM}} \tag{13}$$

$$0 < \rho_1 \le 1 \tag{14}$$

$$0 < \rho_2 \le 1 \tag{15}$$

The design variables ρ_1 and ρ_2 in each finite element control the material properties of PM. Thus, the r and z direction components of the residual flux density $\mathbf{B}_{\mathrm{residual}}$ are defined as

$$B_{\mathrm{residual},r} = B_{\mathrm{residual\_PM}} \cdot \rho_1^3 \cdot \sin\{720^{\mathrm{o}} \cdot (\rho_2 - 0.5)\} \tag{16}$$

$$B_{\mathrm{residual},z} = B_{\mathrm{residual\_PM}} \cdot \rho_1^3 \cdot \sin\{720^{\mathrm{o}} \cdot (\rho_2 - 0.5)\} \tag{17}$$

In (16) and (17), ρ_1 controls the strength of PM, and ρ_2 controls the angle of magnetization direction. A full PM strength $B_{\mathrm{residual\_PM}}$ is fixed as 0.4T in this work.

The objective function (11) is calculated as the RMS value of output voltage $\varepsilon(t)$ in (9):

$$\varepsilon_{\mathrm{rms}} = \sqrt{\frac{1}{T}\int_0^T \varepsilon(t)d(t)} \approx \sqrt{\frac{1}{N}\sum_{j=1}^{N} \varepsilon(t_j)} \tag{18}$$

where the interval T is $2\pi/1000$(Hz).

The finite element formulation of (5) may be represented in matrix form as (12). In (12), **K** and **f** represents the element stiffness matrix and force vector, respectively. In addition, the volume of PM (V_{PM}) can be constrained as V^*_{PM} as shown in (13).

3.2. Design sensitivity analysis

To solve the formulated optimization problem (10)-(15) when using a gradient-based method, the sensitivity of the objectives and constraint functions must be derived.

First, the sensitivity of the objective functions (i.e. the RMS output voltage) can be derived from (9) and (18) as:

$$\frac{d\varepsilon_{\mathrm{rms}}}{d\rho_x} = \left[-\frac{1}{N}\sum_{j=1}^{N}\left\{\left[\sum_i \frac{L_i(x(t_j))}{dx}\Phi_i\right]\cdot \omega X \cos\cos(\omega t_j - \phi)\right\}\right]^{-\frac{1}{2}}$$

$$\times \left[-\frac{1}{N}\sum_{i=1}^{N}\left\{\left[\sum_i \frac{L_i(x(t_j))}{dx}\frac{d\Phi_i}{d\rho_x}\right]\cdot \omega X \cos\cos(\omega t_j - \phi)\right\}\right] \tag{19}$$

This result requires the evaluation of $d\Phi_i/d\rho_x$, which is analytically, derived using the adjoint variable method [22]. The flux linkage Φ_i with adjoint term may be written as:

$$\Phi_i = \Phi_i(A_\theta) + \lambda_i^T[\mathbf{K}_i(\rho_1)\mathbf{A}_{\theta,i} - \mathbf{f}_i(\rho_1,\rho_2)] \tag{20}$$

where λ_i is the adjoint variable. The sensitivity of (20) with respect to ρ_1 and ρ_2 is derived as:

$$\frac{d\Phi_i}{d\rho_1} = \frac{\partial\Phi_i}{\partial\rho_1} + \lambda_i^T\left[\frac{\partial\mathbf{K}_i(\rho_1)}{\partial\rho_1}\mathbf{A}_{\theta,i} - \frac{\partial\mathbf{f}_i(\rho_1,\rho_2)}{\partial\rho_1}\right] \tag{21}$$

$$\frac{d\Phi_i}{d\rho_2} = \frac{\partial\Phi_i}{\partial\rho_2} - \lambda_i^T\left[\frac{\partial\mathbf{f}_i(\rho_1,\rho_2)}{\partial\rho_2}\right] \tag{22}$$

The adjoint variable λ_i is then obtained by solving the adjoint equation derived as:

$$\mathbf{K}_i(\rho_1)^T\lambda_i = -\frac{\partial\Phi_i}{\partial A_\theta} \tag{23}$$

The term $\partial\Phi_i/A_\theta$ in (23) can be calculated from (6). Through (19)-(23), the sensitivity of the objective function can be obtained. The sensitivity of the constraint function (13)-(15) is easily derived because they are linear, and thus, do not need to be explained here.

4. Optimization Results

The proposed optimization method is applied for the design of PM in vibration energy harvester model shown in Fig. 5. Firstly, the optimization is performed with fixed magnetization direction and volume of PM. Then, the optimal shape with four different magnetization directions without the volume constraint is being provided. Finally, both magnetization direction and PM locations are optimized without the volume constraint. To represent the oscillation of mass, the coil moves by 6mm downward, instead of design domain movements for simple implementations. The optimal design is found by solving the optimization problem (10)-(15) when using a Method of Moving Asymptotes (MMA) [23].

4.1. Upward magnetization direction with volume constraint

First, the proposed method is applied when the magnetization direction of PM is fixed upwards (i.e. constant ρ_2) and volume constraint V^*_{PM} is set to be 40%, which is the same as the magnetization direction and the volume of initial design in Fig. 2.

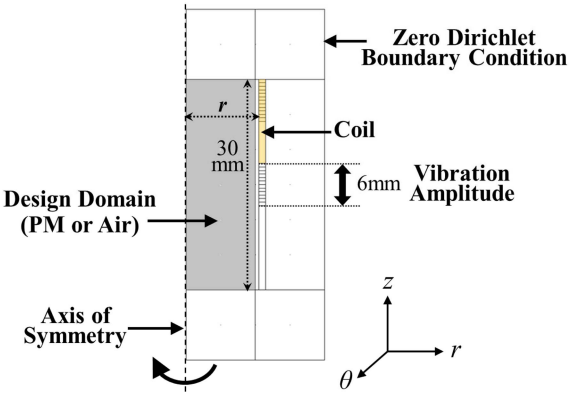

Fig. 5. (Color online) Design domain and analysis domain with boundary condition.

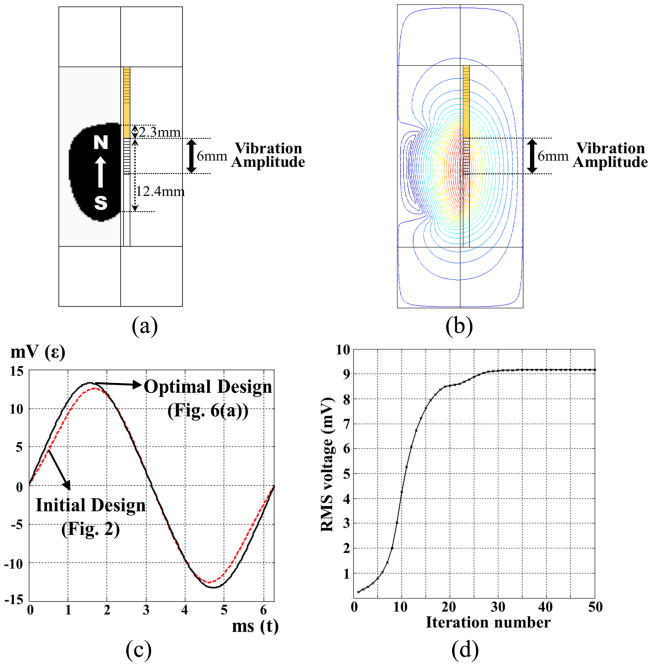

Fig. 6. (Color online) Optimization result (upward magnetization direction, 40% volume constraint): (a) Optimal PM, (b) Magnetic field distribution, (c) RMS output voltage comparison with initial design, (d) objective function history.

The proposed method successfully finds the optimal design of PM by maximizing the output voltage as shown in Fig. 6(a). The optimal design of PM is located between 2.3 mm higher to 12.4 mm lower from the coil bottom location. Fig. 6(b) shows the magnetic field distributions of the optimal design. The optimal PM design maximizes the time variation of the flux linkages, and consequently increases the output voltage as shown in Fig. 6(c). The RMS value of output voltage in optimal design is predicted as 9.156 mV, which is 10.8% higher than that of the initial design (8.503 mV). The convergence history of the objective function is shown in Fig. 6(d). The volume constraint was satisfied during the optimization.

4.2. Fixed magnetization direction without volume constraint

The optimization results from different PM magnetization directions are compared herein. The optimization process was performed for four fixed PM magnetization directions (0°, 45°, 90° and 135° with respect to z-axis). That is, the ρ_2 is fixed as constant for 0.5, 0.5625, 0.625 and 0.6875, respectively. The volume of PM is not being constrained to observe the maximum performances regardless of the PM amount. After performing the optimization with volume constraints, it is observed that there exists the optimal PM volume which maximizes the performance for each magnetization directions. The optimal PM volume can be found by optimization without volume constraints. Fig. 7(a)-(d)

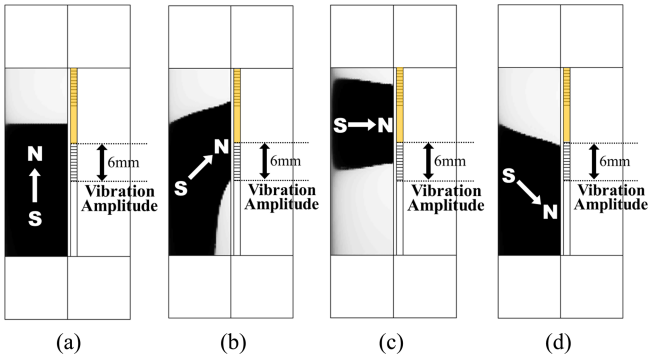

Fig. 7. (Color online) Optimization result for different PM magnetization directions: (a) 0°, (b) 45°, (c) 90° (d) 135°

Table 1. Comparison of volume and RMS voltage

Magnetization angle to z-axis	Volume (%)	RMS Voltage (mV)
0° (Fig. 7(a))	71.72	10.101
45° (Fig. 7(b))	71.13	8.052
90° (Fig. 7(c))	50.87	5.799
135° (Fig. 7(d))	65.52	7.531

show the optimization results in each magnetization direction. The design which maximizes the RMS output voltage is obtained for each case. Table 1 compares the volume and RMS voltage of each optimization result. It also shows that the optimization result for 0° (Fig. 7(a)) generates the largest RMS voltage.

4.3. Optimization of Magnetization Direction

The optimization process is performed by including the design of the magnetization direction for each finite element. That is, both ρ_1 and ρ_2 are optimized as design variables without volume constraints. The PM design results and its magnetic field distributions are shown in Fig. 8(a) and (b). The volume of PM is 99.63%, which means that the design domain is almost filled with PM material. In the optimization result, the PM magnetization direction continuously varies upwards and downwards. The RMS output voltage of the optimal design is expected to be 19.599 mV, which is 230.48% higher than that of the initial design in Fig. 2 (8.503 mV). Although the PM amount of optimal design (99.63%) is much larger than that of the initial design (40%), the huge improvement by optimization is mainly achieved by optimizing the magnetization direction. When the magnetization direction is fixed, the 100% PM volume may result in zero output voltage. The PM volume might be considered as one of the design variables combined with the magnetization direction.

The continuous variation of the magnetization direction in optimal PM design is not available in terms of fabrication. Based on the optimization result, the magnetization

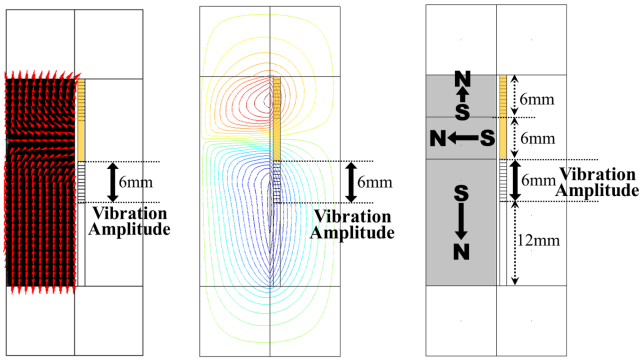

Fig. 8. (Color online) Optimization result (Magnetization direction design): (a) PM design result (arrow shows the magnetization direction), (b) magnetic field distribution, (c) Simplified PM design.

direction is simplified into three directions (i.e. upwards, leftwards, and downwards) as shown in Fig. 8(c). The RMS voltage of this simplified design is calculated as 18.723 mV, which is still higher (220.20%) than the initial design. This result confirms that the PM combination with different magnetization directions can generate much higher output voltages as compared to those using PM with single magnetization directions.

5. Conclusion

An electromagnetic energy harvester was designed by using the topology optimization approach. The optimal shapes and locations of the PM were designed to maximize the RMS values of output voltage. The combination of PM with three different magnetization directions is expected to generate much higher voltage than the harvester when using the PM with single magnetization direction. In the future, the coil shapes and locations can be co-designed for better performances. In addition, the proposed methods may be applied to the other types of energy harvesters including back iron materials, which can also be co-designed.

Acknowledgment

This work was supported by 2012 Korea Aerospace University Faculty Research Grant.

References

[1] S. P. Beeby, M. J. Tudor, and N. M. White, Meas. Sci. Technol. **17**, 12 (2006).
[2] S. Roundy, P. K. Wright, and J. Rabaey, Comput. Commun. **26**, 1131 (2003).
[3] H. Kulah and K. Najafi, IEEE Sensors Journal **8**, 261 (2008).
[4] B. Yang, C. Lee, W. Xiang, J. Xie, J. H. He, R. K. Kotlanka, S. P. Low, and H. Feng, J. Micromech. Microeng. **19**, (2009).
[5] T. Jirku, P. Fiala, and M. Kluge, Microsyst. Technol. **16**, 677 (2010).
[6] I. Sari, T. Balkan, and H. Kulah, Sensors Actuat. A-Phys. **145**, 405 (2008).
[7] C. L. Zhang and W. Q. Chen, Appl. Phys. Lett. **96**, 123507 (2010).
[8] T. Galchev, H. Kim, and K. Najafi, Proceeding of International Solid-State Sensors, Actuators and Microsystems Conference, Denver, CO, USA (2009).
[9] V. R. Challa, M. G. Prasad, Y. Shi, and F. T. Fisher, Smart Mater. Struct. **17**, 015035 (2008).
[10] Z. Hadas, C. Ondrusek, and V. Singule, Microsyst. Technol. **16**, 691 (2010).
[11] X. Xing, J. Lou, G. M. Yang, O. Obi, C. Driscoll, and N. X. Suna, Appl. Phys. Lett. **95** 134103 (2009).
[12] M. P. Bendsøe and O. Sigmund, Topology Optimization - Theory, Methods and Applications, 2nd ed., Springer, Berlin (2004).
[13] S. Park and S. Min, IEEE Trans. Magn. **45**, 5 (2009).
[14] J. Lee, E. M. Dede, and T. Nomura, IEEE Trans. Magn. **47**, 12 (2011).
[15] J. S. Choi, IEEE Trans. Magn. **47**, 10 (2011).
[16] B. Zheng, C.-J. Chang, and H. C. Gea, Struct. Multidiscip. O. **38**, 1 (2009).
[17] J. S. Choi and J. Yoo, Comput. Methods in Appl. Mech. Eng. **198**, 27 (2009).
[18] J. Lee, T. Nomura, and E. M. Dede, Appl. Phys. Lett. **101**, 123507, 2012.
[19] D. Spreemann, D. Hoffmann, B. Folkmer, and Y. Manoli, J. Micromech. Microeng. **18**, 104001 (2008).
[20] D. Spreeman, and Y. Manoli, Electromagnetic Vibration Energy Harvesting Devices, Springer (2012).
[21] E. M. Yeatman, Proc. IMechE Part C: J. Mechanical Engineering Science **222**, 1 (2008).
[22] L. H. Olesen, F. Okkels, and H. Bruus, Int. J. Numer. Methods Eng. **65**, 975 (2006).
[23] K. Svanberg, Int. J. Numer. Methods Eng. **24**, 359 (1987).